Review and Analysis

Alan W. Rempel*

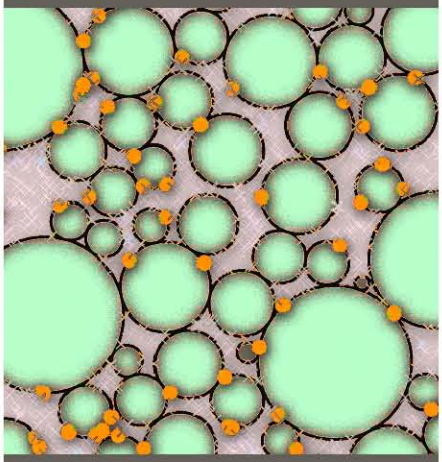

The saturation behavior of partially frozen soils is affected by pore geometry, wetting interactions, and the colligative effects of solutes. The wetting interactions between pore ice and the sediment matrix also produce the net thermomolecular force that causes frost heave. For illustration, the saturation behavior and thermomolecular force are quantified using a simple, two-dimensional, model porous medium in a series of Monte Carlo simulations.

Dep. of Geological Sciences, Univ. of Oregon, Eugene, OR 97403. *Corresponding author (rempel@uoregon.edu).

Vadose Zone J.
doi:10.2136/vzj2012.0045
Received 3 Apr. 2012..

Hydromechanical Processes in Freezing Soils

The study of freezing in soils has benefited immensely from analogies with physical processes that take place within the unsaturated zone. The surface energies and wetting interactions that produce differences in pressure between the pore-filling phases cause a qualitatively similar saturation dependence on geometrical characteristics, such as the pore size distribution. The ability of solid ice surfaces to support shear tractions contrasts with the fluidity of air, however, and the limited need for transport on solidification is notably different from the wholesale displacement of gas and liquid volumes that is necessary to change saturation levels in the vadose zone. This brief review outlines the main points of common ground and some of the essential differences that separate partially frozen and unsaturated soils. Particular attention is paid to an illustration of the ice and liquid saturation behavior in a two-dimensional model porous medium, both in a pure water system and with solutes present at a specified (bulk) concentration relative to the total mass of pore constituents. A derivation is developed for the net thermomolecular force exerted by sediment particles on an ice lens, and the model soil parameters are used to examine how the colligative effects of impurities modify the loads that can be supported in this way. The focus of this study is on describing and quantifying the physical interactions that underlie the vast range of hydro-mechanical processes in freezing soils.

When sediments that contain liquid water are cooled below freezing, the dynamics of solidification give rise to a wide range of interesting and peculiar phenomena. Arrays of vertically oriented crystals, known as *needle ice*, grow at the ground surface and delicately support pebbles and small clods of soil (Lawler, 1988). Rocks in fields and artifacts at archeological sites are pushed upward, past the surrounding fine-grained material (Anderson, 1988). Under the more hostile conditions found in polar regions and even on the surface of Mars, semi-regular polygons of raised and lowered earth form patterned ground (e.g., Hallet, 1990; Peterson and Krantz, 2008; Mangold et al., 2004). Infrastructure costs mount from the cracks and potholes that develop in road surfaces and damage to building foundations by frost heave that results when macroscopic ice lenses grow by drawing water up from below (e.g., Andersland and Ladanyi, 2004). The very same physical interactions determine the basal geometry and depth of "freeze-on" beneath soft-bedded glaciers (Rempel, 2008), which in this sense might be thought of as the most spectacular ice lenses on our planet. All of this behavior is traced to slight modifications in the equilibrium phase behavior that are induced by characteristics of the soil and its interactions with liquid water and solid ice (e.g., Dash, 1989; Dash et al., 2006).

Historical Notes

Early investigators of needle ice recognized that the volumetric expansion associated with the density difference between liquid water and ice is inadequate to explain these transient features (Abbe, 1905; Le Conte, 1850). Instead, as Le Conte (1850, p. 34) observed, "even on those portions of the soil, where the phenomenon does not manifest itself ... the amount of moisture found at the surface of the ground *after* a thaw, is vastly greater than was present *before* congelation took place." A comprehensive field and laboratory study of sediments that are susceptible to frost heave and the accumulation of such excess moisture led Beskow (1991) to argue that capillary interactions probably play a role. Experiments by Taber (1929, 1930) highlighted the importance of thin liquid films for transport between growing ice crystals and the host sediment particles. Taber also demonstrated convincingly that the volume increase on freezing a fixed water mass is of minimal importance by showing that similar lensing phenomena occur in substances (benzene and nitrobenzene) that contract on freezing.

Throughout the early and mid-20th century, expanding economic and cold-war interest in the arctic intensified research efforts, many of which were summarized by Black (1991). Gilpin (1980) presented one of the first reasonably complete mathematical models to appear in the western literature describing the supply of liquid to growing ice lenses through a partially frozen "soil" comprised of stacked uniform spheres; inside the pore space, small amounts of residual liquid remain in equilibrium with ice because of wetting interactions at particle surfaces and the effects of surface energy, which depress the melting temperature where the ice–liquid interface is highly curved. Considering these same physical ingredients and building on earlier work (Miller, 1978; Miller and Koslow, 1980), O'Neill and Miller (1985) developed a continuum description of frost heave that uses empirical parameterizations for the dependence of ice saturation and permeability on temperature in a partially frozen fringe through which liquid flows to supply the active lens until a new lens initiates and begins to grow.

Advances in the theory of premelting have provided new insights into the physical mechanisms that underlie frost heave and related phenomena (e.g., Dash, 1989; Dash et al., 2006). *Premelting* is the term used to describe the presence of a liquid-like phase in equilibrium with the solid phase below the normal bulk melting temperature, which is the temperature that would pertain in a system with the pure solid and liquid in contact along a planar interface that is outside the range of intermolecular interactions with any other substance (i.e., 0°C for ice and water at atmospheric pressure). Experiments by Wilen and Dash (1995) showed that, despite the fact that surface-energy effects are responsible for most of the liquid contained in partially frozen soils across a substantial and relevant temperature range (see below), liquid transport has a different physical origin from the capillary rise that occurs in the unsaturated zone. Instead, the net thermomolecular force that opposes gravity to enable frost heave and cause liquid flow is due solely to the intermolecular forces that give rise to the thin premelted films that wet the interface between soil particles and ice (Rempel et al., 2001). This insight has since been incorporated within continuum treatments that account for the thermomolecular force by rigorously coupling ice saturation to the force balance conditions that control both lens initiation and subsequent growth (e.g., Rempel et al., 2004). An alternative mechanism for ice-lens initiation that was recently proposed also relies on the thermomolecular force that acts between the ice and mineral particles and highlights the importance of inhomogeneities in the pore-size distribution. Surface-energy effects dictate that ice is able to form in the largest pores first, and subsequently the thermomolecular force can produce a new lens by enabling ice growth to propagate a crack, without requiring that a preexisting frozen fringe connect it to an overlying lens, as previous models had assumed (Style et al., 2011). Indeed, the dominant cause of frost damage to cohesive materials in many natural and laboratory settings can also be traced to premelted liquid transport that supplies ice growth to propagate cracks (e.g., Hallet, 2006; Murton et al., 2006).

Overview

The physical interactions that control the behavior of ice and liquid water in partially frozen soils have much in common with the physical interactions that control the behavior of air and liquid water in the unsaturated zone. In both cases, the surface energy of the interface between the two phases and the wetting characteristics of the soil particles modify the conditions for equilibrium and produce a pressure difference across the phase boundary. In partially frozen soils, this pressure difference is directly proportional to the temperature depression, or *undercooling*, below the normal bulk melting point. The next section, on equilibrium phase behavior, describes efforts to account for the dependence of saturation on undercooling in soils with different geometrical and surface characteristics. A subsection on ice saturation in a two-dimensional porous medium describes Monte Carlo simulations used to calculate the liquid saturation and illustrate these controls, as well as the importance of colligative effects when dissolved impurities are present. In the unsaturated zone, the low viscosity and density of air in comparison with liquid water ensure that the air pressure is nearly uniform throughout and equal to atmospheric levels. The situation in partially frozen soils is quite different because liquid is much more readily deformed than solid ice. Pressure gradients can persist within the ice and this affects the manner in which liquid is transported. The controls on liquid flow and some of the implications for dynamic processes are discussed in a separate major section on premelting dynamics, again using the simple model soil as a reference case.

This review focuses on aspects of the physics of freezing in soils that share similarities with behavior in the unsaturated zone but also some notable differences. Although the scope of the discussion is necessarily limited, the intention is to summarize enough of the background physics to provide an entry into some of the more interesting challenges that remain topics of active research.

Equilibrium Phase Behavior

The partitioning of pore volume between liquid water and ice has been the subject of numerous experimental investigations, in large part motivated by geotechnical considerations including the influence on heat flow, liquid transport, and ground deformation (e.g., Andersland and Ladanyi, 2004). When a saturated soil is cooled, ice first reaches equilibrium with the surrounding pore liquid once the temperature, T, drops lower than the normal bulk melting temperature, T_m (i.e., 0°C at atmospheric pressure for pure water; changes in T_m with pressure are described by the Clausius–Clapeyron relation) to achieve a finite undercooling $\Delta T_f = T_m - T$. Field and laboratory measurements have confirmed that ΔT_f scales with the typical pore size, as expected from the way in which the ice–liquid surface energy, γ_{il}, influences the equilibrium behavior. With geometrical restrictions permitting the principal radii of curvature of the largest ice grains to reach the pore radius R_p, the

Gibbs–Thomson effect predicts that $\Delta T_f \approx 2\gamma_{il} T_m / \rho_i L R_p$, where ρ_i is the ice density and L is the latent heat of fusion.

The surface energy of the ice–liquid interface is clearly important for determining the geometry (i.e., curvature) of the phase boundary, but the wetting interactions that promote the coexistence of the premelted liquid films that separate the ice and soil particle surfaces arise from intermolecular interactions among all three components. Gilpin (1979) assumed a simple power-law relationship between film thickness d and undercooling $\Delta T = T_m - T$. While the decrease in d as ΔT increases can be much more complicated, detailed treatments (e.g., Israelachvili, 1992; Wettlaufer, 1999) have revealed circumstances in which either a power-law or an exponential relationship does give a reasonable approximation. For example, in the common situation where mineral particles have charged surfaces that cause ordering among a dilute concentration of cations and anions in the liquid film, a net entropic repulsion develops between the ice and the mineral particles with the strength of the "disjoining" pressure $\Pi \approx P_0 \exp[(\lambda_0 - d)/\lambda_d]$, where the decay distance λ_d is identified with the Debye length (e.g., Israelachvili, 1992) and λ_0 is the film thickness at which $\Pi = P_0$, a reference pressure. In circumstances where such "double-layer forces" are less important, induced dipole interactions can lead to $\Pi \approx P_0(\lambda_0/d)^3$; similar expressions with different exponents are more appropriate in other cases (e.g., Wettlaufer et al., 1996). Irrespective of the molecular-scale origins and functional form of $P(d)$, the relationship to the equilibrium undercooling against a planar interface gives $\Delta T \approx T_m \Pi(d)/\rho_i L$. In the more general case, where the mean curvature κ of the ice–liquid interface is non-zero, the combination of effects implies that (e.g., Rempel et al., 2001)

$$\rho_i L \frac{\Delta T}{T_m} \approx \gamma_{il}\kappa + \Pi(d) \qquad [1]$$

In principle, d and κ give sufficient geometrical information to describe the equilibrium shape of any ice–liquid phase boundary, with Eq. [1] describing their dependence on ΔT. In the simple example where spherical ice grains have $k = 2/R_p$ and d is large enough that $\Pi(d) << \gamma_{il}\kappa$, ice and liquid first coexist at equilibrium with $\Delta T = \Delta T_f$. As ΔT increases further (e.g., as T drops), Eq. [1] continues to describe how κ increases and d shrinks to enable the saturation level of ice within the pore space S_i to rise.

Inferring Ice Saturation Behavior from Drying Behavior

By equating the chemical potentials in the two phases, it is easy to show that the temperature offset from bulk equilibrium conditions, ΔT, also implies a pressure difference between the solid ice P_i and the liquid water P_l, such that $P_i - P_l \approx \rho_i L \Delta T / T_m$ (e.g., Dash et al., 2006). The coefficient $\rho_i L/T_m \approx 1.1$ MPa/°C, so the undercooling need not be very high to generate a reasonably large magnitude of $P_i - P_l$. A nearly identical relationship to Eq. [1] can be used to describe the "matric potential," or the pressure difference between the vapor P_v and liquid P_l phases in unsaturated media so that (e.g., Or and Tuller, 1999; Rascón and Parry, 2000)

$$P_v - P_l \approx \gamma_{vi}\kappa + \Pi_v(d) \qquad [2]$$

where γ_{vl} is the surface energy (or surface tension) of the vapor–liquid interface and the subscript v in the second term on the right is used to emphasize that the important wetting interactions for this case involve intermolecular forces between the substrate, liquid, and vapor molecules. The close analogy between partially frozen and partially vapor-saturated media suggests the potential to infer the ice saturation, S_i, as a function of undercooling based on measurements of the vapor saturation, S_v, as a function of $P_v - P_l$ in the same soil. At sufficiently low interphase pressure differences, most of the liquid volume is present because of surface-energy effects (i.e., in locations where the second terms on the right side of both Eq. [1] and [2] are negligible), so the ratio $\gamma_{vl}/\gamma_{il} \approx 2.2$ can be used to scale the results of unsaturated experiments and apply them to the partially frozen case (see discussions by O'Neill, 1983; O'Neill and Miller, 1985). At larger $P_v - P_l$ (or $P_i - P_l$), however, the films coating sediment particles contain an increasing proportion of the remaining liquid volume (discussed further below). The differences between the strengths and nature of the dominant wetting interactions that are embodied in the functions $\Pi(d)$ and $\Pi_v(d)$ are difficult to quantify, implying that unsaturated experiments on their own are less reliable for predicting saturation levels in partially frozen soils at high ΔT, as illustrated by the calculations for a two-dimensional model porous medium below. By combining measurements of specific surface area with the results from unsaturated experiments, the dependence of film thickness on $P_v - P_l$ can be inferred and scaled separately in systems where the interfacial premelting behavior is understood, but such a strategy has not seen wide use.

Ice Saturation Calculations in Idealized Systems

If enough is known about the surface properties, shapes, and packing arrangement of particles that form a porous medium, it is possible to use Eq. [1] to calculate how the ice saturation changes as a function of undercooling. This is the approach taken by Cahn et al. (1992), who considered idealized packings (face-centered cubic and body-centered cubic) of identical spherical particles. Following a correction noted by Dash et al. (2006), the theoretical predictions for $S_i(\Delta T)$ are in excellent agreement with the interpretation of quasi-elastic neutron scattering data from experiments in monodispersed graphite and talc powders (Maruyama et al., 1992). Measurements of ice saturation in graphite sheets (Gay et al., 1992) and porous silica glass (Ishizaki et al., 1996) also compare favorably with theoretical predictions in the large undercooling limit, when most of the liquid is contained within premelted films where the second term on the right side of Eq. [1] dominates. The complications that arise when ionic impurities are present and the intermolecular forces that contribute to determining $\Pi(d)$ are varied in nature have been explored

in detail for monodispersed, random-close-packed spheres of fused quartz, gold, and silicon in a theoretical treatment by Hansen-Goos and Wettlaufer (2010); that work also highlighted the important contribution of the liquid fraction contained in veins that ring the grain boundaries between adjacent ice crystals.

Natural porous media are comprised of particles with wide ranges of sizes and shapes, variations in surface characteristics that complicate the wetting properties, and small concentrations of soluble impurities that can significantly alter equilibrium behavior. Empirical data that describe the variation of S_l with DT in particular soils are invaluable inputs for quantitative models of freezing behavior and associated hydromechanical phenomena. The required data are limited, however, and there remains a need for more sophisticated treatments that can predict how different soil characteristics will affect the saturation behavior under more varied circumstances. It is difficult to directly solve Eq. [1] for the detailed surface geometry of the ice–liquid interface (i.e., κ and d) throughout more realistic sediments, but fortunately, computational resources now make alternative strategies feasible.

Ice Saturation in a Two-Dimensional Model Porous Medium

Figure 1 shows a 20- by 25-μm section of a model porous medium that was constructed by packing together 5000 circular particles chosen from a lognormal distribution with mean radius 1 μm and variance 0.5 μm^2. For the purposes of illustration, the kinetics of ice nucleation are ignored and it is assumed that matrix particles are completely wetted by the liquid phase in preference to ice; in other words, complete premelting takes place (Dash et al., 2006). At any given point within the pore space, the phase change from liquid water to ice will take place at a particular undercooling that is associated with one of three scenarios:

1. If the point is close enough to the pore center, the phase change will take place once ice is first able to form in the pore at a threshold undercooling that allows a circular crystal to barely fit between the adjacent particles.
2. If the chosen point is far enough from both the pore center and the pore walls, it can remain in the liquid after pore ice first forms, with equilibrium instead being reached once it is cold enough for κ to become sufficiently large.
3. If the point is close enough to one of the particle surfaces along a pore wall, it can instead be part of the premelted film up until d thins sufficiently at a particular undercooling.

To determine how the liquid saturation level changes with undercooling in the model soil, 100,000 points were chosen at random and the undercooling needed to reach equilibrium was evaluated for each location. Points that last remained in the liquid phase because of surface-energy, or "capillary," effects (i.e., Scenarios 1 and 2) are marked in Fig. 1 by light gray crosses, while those that were contained within premelted films immediately before freezing (Scenario 3) are shown with filled circles.

Evaluating the undercooling needed for equilibrium at a large number of points and compiling the results gives the statistical

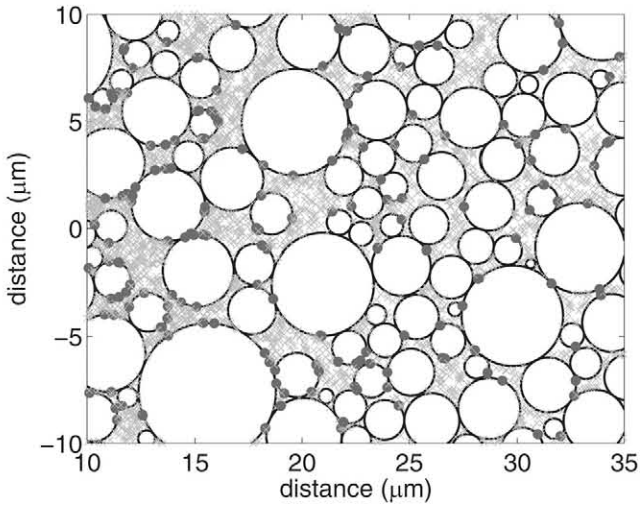

Fig. 1. A portion of a two-dimensional porous medium that consists of a lognormal distribution of circular particles characterized by a mean radius of 1 μm and a variance of 0.5 μm^2 (mode 0.54 μm, median 0.82 μm). Light gray crosses mark randomly chosen points where ice first forms from residual liquid with an undercooling attributed to surface-energy (curvature) effects. Filled circles are points where the last remaining liquid is in premelted films that separate ice from the nearby particle surfaces.

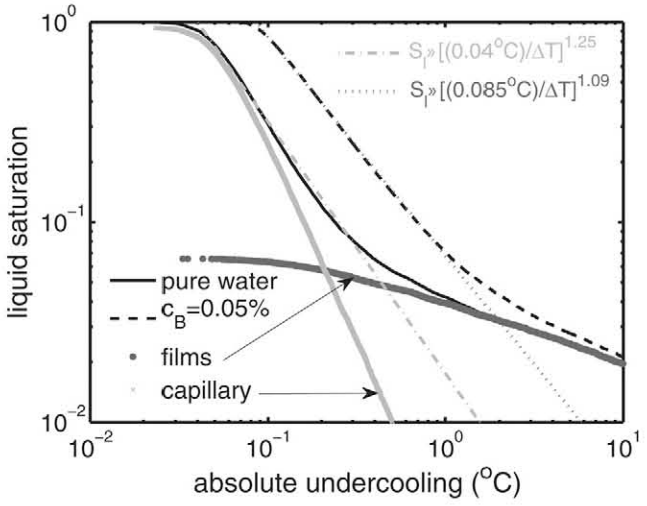

Fig. 2. Liquid saturation S_l as a function of undercooling ΔT obtained from Monte Carlo simulations on the porous medium displayed in Fig. 1. On the left, the black solid line shows the total liquid saturation calculated from the cumulative sum of the liquid sampled by points marked with light gray crosses in Fig. 1, which represent regions where equilibrium is limited by the high curvature of the ice–liquid interface, and the filled circles in Fig. 1, which represent the residual liquid that is contained within premelted films. The dot-dashed line is a power-law fit to saturation values between 5 and 90%. On the right side of the graph, the dashed curve shows the expected saturation behavior when a salt solution with bulk concentration c_B = 0.05% (w/w) is present, while the dotted line traces the corresponding power-law fit.

estimate of the change in liquid saturation with undercooling that is shown with the solid black line in Fig. 2. Light gray crosses mark the undercooling at which the interfacial curvature first allows ice to be in equilibrium with the pore liquid at one of the sampled points (see Fig. 1). The total liquid saturation and the trend traced by the gray crosses correspond closely with each other at first because surface-energy effects are responsible for most of the liquid that is present at low undercoolings (i.e., $\Delta T < 0.2$°C here). The filled circles show the undercooling at which ice first reaches equilibrium with the pore liquid along the boundary of a premelted film (see Fig. 1). For illustrative purposes, in these calculations the equilibrium undercooling in the premelted films is assumed to satisfy [i.e., from Eq. [1] with $\kappa = -1/R_i$ and $\Pi = P_0(\lambda_0/d)^3$]

$$\Delta T_{film} \approx \frac{T_m}{\rho_i L}\left[P_0\left(\frac{\lambda_0}{d}\right)^3 - \frac{\gamma_{il}}{R_i}\right] \quad [3]$$

where R_i is the radius of the nearest particle, and the wetting interactions imply a film thickness of $d = \lambda_0 = 10$ nm along a planar interface when the disjoining pressure is $\Pi = P_0 = 1.1$ MPa. With the model parameters chosen here, the premelted films make a significant contribution to the total liquid volume when $\Delta T \approx 0.1$°C and $S_l \approx 0.3$, and the film volume exceeds the volume present because of surface-energy effects once $\Delta T > 0.2$°C and $S_l < 0.1$ (i.e., at the undercooling where the filled circles and gray crosses meet on Fig. 2). As noted above, because the wetting interactions that cause liquid films to coat soil particles in the unsaturated zone are different from those that cause premelted films to separate soil particles from pore ice (i.e., the former involve intermolecular forces between particles, liquid, and vapor, whereas the latter involve intermolecular forces between particles, liquid, and ice), this suggests that attempts to infer the ice saturation behavior using measurements under unsaturated conditions diminish in value when $S_l < 0.3$ (in a soil with the characteristics chosen for this model).

Power-Law Approximations for the Dependence of Saturation on Undercooling

Empirical measurements of liquid saturation S_l in partially frozen porous media are made across a limited range of conditions, and reported power-law fits for the corresponding ice saturation $S_i = 1 - S_l$ in the form

$$S_i \approx 1 - \left(\frac{\Delta T_f}{\Delta T}\right)^\beta \quad [4]$$

are used in many continuum treatments of hydromechanical processes (e.g., O'Neill and Miller, 1985; Andersland and Ladanyi, 2004). The dot-dashed line in Fig. 2 shows the best power-law fit to the synthetic liquid saturation data across a range from 5 to 90%, which satisfies Eq. [4] with $\Delta T_f \approx 0.040$°C and $\beta \approx 1.25$. From the form of the solid black curve in Fig. 2, it is clear that both the exponent β of the best power-law fit and the intercept $D T_f$ with $S_l = 1$ are smaller when the range of saturation levels that is considered has lower values and the contribution from premelted films is more prominent. (For example, the best power-law fit across a range of S_l from 3 to 75% is characterized by $\Delta T_f \approx 0.036$°C and $\beta \approx 1.09$.) For many natural freezing phenomena, the most interesting dynamic interactions take place when the liquid saturation level is still relatively high, and a simple power-law fit of the form given in Eq. [4] suffices for treating the changes in saturation with undercooling. Nevertheless, it is important to recognize that such a simplification does have limitations and more elaborate parameterizations may be preferable when the range of saturation levels that are encountered cannot be captured by a simple power-law fit (e.g., Watanabe and Wake, 2009). This is particularly important for circumstances involving large thermomolecular forces at high undercoolings and low liquid saturation levels (e.g., the dot-dashed gray and solid black curves diverge significantly for $\Delta T_f > 0.5$°C and $S_l < 5\%$), for example during frost cracking of cohesive materials (e.g., Murton et al., 2006). There are also significant discrepancies right at the onset of ice formation, when some pores contain ice at an undercooling lower than the fitted value of ΔT_f (e.g., note the offset between the intersections of the solid black and dot-dashed gray curves with the upper axis in Fig. 2), which may lead to ice nucleation in disconnected pores, with subsequent lens growth proceeding by a crack-propagation mechanism (e.g., Style et al., 2011).

Colligative Effects of Dissolved Impurities

In natural systems, the water is never pure. Solutes are important both for modifying the strength and form of the intermolecular forces that cause interfacial premelting and for lowering the chemical potential of the liquid, which depresses the melting point. An instructive and practical illustration concerns the case where the slope of the liquidus curve that defines the changes in melting temperature with solute concentration is linear. In this case, the melting temperature along a flat interface that is distant from any foreign substrates can be written as $T_m \approx T_{m0} - \Gamma c$, where c is the solute concentration, T_{m0} is the bulk melting temperature of the pure system, and Γ is the liquidus slope. If the total bulk concentration of solute in the pore space is c_B (defined here as the mass of solute divided by the mass of liquid and ice, but definitions in terms of molarity are equally valid), then because most impurities are efficiently rejected from the ice lattice, the concentration at saturation level $S_l = 1 - S_i$ can be approximated as $c \approx c_B/S_l$, where the small density difference between liquid water ρ_l and ice ρ_i has been neglected for clarity of presentation (more precisely, $c = (c_B/S_l)[S_l + (\rho_i/\rho_l)S_i] \approx c_B/S_l$). Combining the two expressions, we expect that the melting temperature of the bulk solution should depend on the bulk concentration and liquid saturation level according to

$$T_m \approx T_{m0} - \Gamma\frac{c_B}{S_l} \quad [5]$$

With the undercooling redefined as the temperature depression below bulk melting in the pure water system (i.e., the measured

temperature below 0°C in a typical laboratory setup $\Delta T_0 \equiv T_{m0} - T$), Eq. [5] can be substituted into Eq. [1] and rearranged to obtain

$$\Delta T_0 \approx \frac{T_m}{\rho_i L}\left[\gamma_{il}\kappa + \Pi(d)\right] + \Gamma\frac{c_B}{S_l} \qquad [6]$$

The dashed line toward the right side of Fig. 2 shows the predicted saturation from Eq. [6] for a case with $c_B = 0.05\%$ (w/w) and $\Gamma = 0.93°C/\%$ (w/w), which corresponds approximately with the slope of the liquidus for subeutectic aqueous NaCl solutions (eutectic composition 23% by weight, eutectic temperature −21°C). As shown by the dotted gray line, across the range $0.9 > S_l > 0.05$ for this case, the best-fit power law has $\Delta T_f \approx 0.085°C$ and $\beta \approx 1.09$. Note that the focus here has been solely on the colligative effects represented by the final term in Eq. [6]. The effect of solute concentration on the intermolecular forces responsible for interfacial premelting (i.e., by changing the form and strength of Π, as discussed by Wettlaufer, 1999) is neglected in these calculations.

Figure 3 further explores how colligative effects influence the partitioning of pore water between liquid and ice. The black curve shows an approximately linear increase in ΔT_f with c_B once the bulk solute concentration is greater than about 0.2% (w/w). This change in the best-fit relationship coincides with a decrease in the power-law exponent β (shown in red) to a value near unity. The linear decrease in liquid saturation with undercooling that is predicted at high solute concentrations (i.e., leading to $\beta = 1$) is a consequence of the dominant role of the final term on the right-hand side of Eq. [6] in this regime (see also Wettlaufer, 1999).

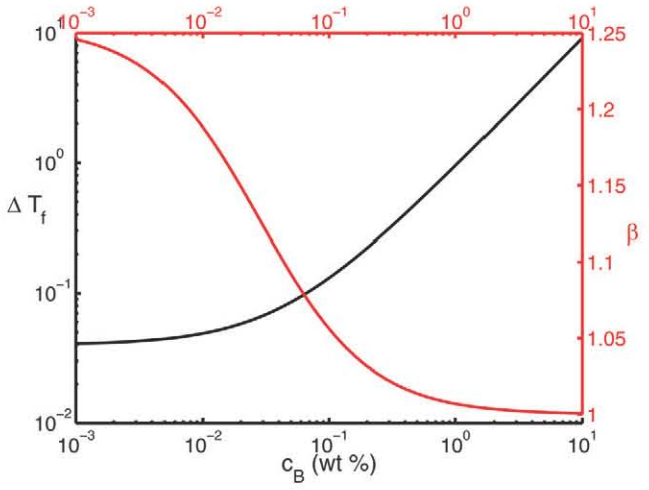

Fig. 3. The best-fit power law parameters in Eq. [4] across the liquid saturation range from 5 to 90%, shown as a function of the bulk concentration of dissolved impurities c_B in the model soil depicted in Fig. 1. The characteristic undercooling ΔT_f is shown in black, with the logarithmic *y* axis on the left. The power-law exponent β is shown in red, with the linear *y* axis on the right.

Additional Considerations

These simple calculations neglect the influence of impurity concentration on the intermolecular interactions that cause premelting, for example in reducing the Debye length that characterizes the range of double-layer forces (see Hansen-Goos and Wettlaufer, 2010). Many other important complications are ignored as well, including: (i) the potential for the kinetics of ice nucleation to cause hysteresis in the saturation behavior during melting and freezing in an analogous way to that associated with gas and liquid transport in the unsaturated zone during imbibition and drainage; (ii) the role of pH and compositional changes in altering the surface properties of mineral particles to affect the wetting and adsorption behavior; (iii) the potential for biological activity to modify the pore environment and the saturation behavior (e.g., Watanabe and Ito, 2008; see also Krembs et al., 2011); (iv) the changes in phase behavior that are associated with the presence of air as a third pore-filling phase (e.g., Watanabe and Wake, 2009); (v) the contribution of premelted liquid along grain boundaries and veins that is particularly important at high crystallinities (e.g., Hansen-Goos and Wettlaufer, 2010); and (vi) the major simplifications in considering a two-dimensional analog for three-dimensional natural systems and approximating particles as smooth circular objects. The saturation behavior can be significantly affected by each of these factors. The strategy used here could be modified to quantify their effects so that the predicted behavior could be compared with the results of controlled laboratory tests. For the present purposes, the essential geometrical controls and colligative effects illustrated above are a sufficient introduction to basic static equilibrium behavior to preface a short overview of premelting dynamics.

Premelting Dynamics

The equilibrium coexistence of liquid water and ice has dynamic consequences when pressure gradients are established to drive liquid flow and when ice–sediment interactions are able to deform the soil matrix. As long as the soil particles are completely wetted by premelted films, there are no contact lines across which capillary forces can be transmitted to cause liquid migration in the manner that occurs in the unsaturated zone. As a consequence, the analysis described below demonstrates that capillary interactions do not themselves generate any net force in partially frozen soils, whether a frozen fringe is present or not. Instead, it is the wetting interactions themselves that produce the net thermomolecular force that acts between the ice and the soil matrix. Because the strength of this force is controlled by thermal conditions, whereas the gravitational load is insensitive to temperature, the distribution of fluid pressures must adjust to satisfy the force balance; this drives liquid flow. The example below illustrates how the thermomolecular force can be determined as a function of undercooling, both when sediments are saturated with pure water and when the colligative effects of dissolved impurities are important. The extent to which similar arguments might find application in unsaturated problems has not been fully explored.

Net Force between Sediment Particles and Ice

Recall that the disjoining pressure $\Pi(d)$ is the force per unit area with which ice and particle surfaces push against each other across the intervening premelted film. To evaluate the total thermomolecular force exerted by the wetted particles on an ice–liquid surface S, Eq. [6] can be used to write

$$\begin{aligned}\mathbf{F}_T &= -\int_S \Pi(d)\,\mathrm{d}\mathbf{S} \\ &\approx -\int_S \left[\frac{\rho_i L}{T_m}\left(\Delta T_0 - \Gamma\frac{c_B}{S_l}\right) - \gamma_{il}\kappa\right]\mathrm{d}\mathbf{S}\end{aligned} \quad [7]$$

For the case of a flat ice–liquid surface, the curvature is zero, and if the surface is oriented so that the temperature offset from bulk melting at the local impurity concentration is constant (e.g., along an isotherm), then Eq. [7] simplifies to give

$$\begin{aligned}\mathbf{F}_T &= -\frac{\rho_i L A}{T_m}\hat{\mathbf{n}}\left(\Delta T_0 - \Gamma\frac{c_B}{S_l}\right) \\ &= -\frac{\rho_i L A}{T_m}\hat{\mathbf{n}}\left(T_m - T\right)\end{aligned} \quad [8]$$

where A is the cross-sectional area, $\hat{\mathbf{n}}$ is the unit outward normal to the ice surface, and Eq. [5] is used to arrive at the final expression on the right. Over any closed ice–liquid surface, the integral of the curvature vanishes (i.e., $\int_S \kappa\,\mathrm{d}\mathbf{S} = 0$) so that, treating γ_{il} as constant, for this case Eq. [7] can be transformed to the integral over the enclosed volume V as

$$\begin{aligned}\mathbf{F}_T &= -\int_V \nabla\left[\frac{\rho_i L}{T_m}(T_m - T)\right]\mathrm{d}V \\ &\approx \frac{\rho_i L}{T_{m0}}\int_V \mathbf{G}\,\mathrm{d}V\end{aligned} \quad [9]$$

where the approximation that $\rho_i L/T_m \approx \rho_i L/T_{m0}$ has been used to simplify the final expression on the right. For example, when the gradient $\mathbf{G} = \nabla(T - T_m)$ is constant throughout the volume, this implies that $\mathbf{F}_T = (L\mathbf{G}/T_{m0})m_i$, where m_i is the mass of ice that could fit within the volume. The dependence on ice mass and a thermodynamic potential gradient suggests that $\mathbf{F}_T$ be thought of as a kind of "thermodynamic buoyancy force" (Rempel et al., 2001). Together, Eq. [8] and [9] can be combined to evaluate the force exerted by sediments on a geometrically complex ice surface, such as is expected to sometimes extend from a growing lens into the adjacent partially frozen sediments (e.g., Rempel et al., 2004). To derive a closed-form expression, it is useful to assume a linear liquidus and the power-law saturation behavior given by Eq. [4]; both of these approximations are easily generalized, however, starting from the final expressions given in Eq. [8] and [9].

Thermodynamic Buoyancy with Impurities

Most published treatments of frost heave and related premelting dynamics have focused on idealized cases where the effects of impurities were neglected so that $c_B = 0$, $T_m = T_{m0}$ is constant, and $\mathbf{G} = \nabla T$. When T_m changes across the relevant volume because of colligative effects, the gradient $\mathbf{G}$ is no longer equal to the temperature gradient, but instead it is the gradient in the amount by which the temperature is offset from the bulk equilibrium temperature at the local solute concentration; this is precisely the offset attributed to the effects of wetting interactions and curvature. Because the force integral in Eq. [9] is over a volume that invariably depends in some way on the ice saturation, it is useful to write S_i as a function of the offset from bulk melting at the local solute concentration $T_m - T$ as well, rather than the offset from bulk melting in the absence of impurities $T_{m0} - T$. For the Monte Carlo simulations of saturation behavior discussed above, Fig. 3 shows how the impurity content c_B affects the exponent β and characteristic undercooling ΔT_f in a power-law fit to saturation data of the form given in Eq. [4]. In the saturation regime where the influence of impurities on the strength of the wetting interactions is much less important than colligative effects throughout the liquid volume, this relationship may be expressed as

$$\begin{aligned}S_i &\approx 1 - \left(\frac{\Delta T_f}{\Delta T_{m0}}\right)^{\beta} \\ &\approx 1 - \left(\frac{\Delta T_{f0}}{T_m - T}\right)^{\beta_0}\end{aligned} \quad [10]$$

where ΔT_{f0} and β_0 are the best-fit parameters in the absence of impurities (e.g., given approximately by the low-c_B limit on the left side of Fig. 3).

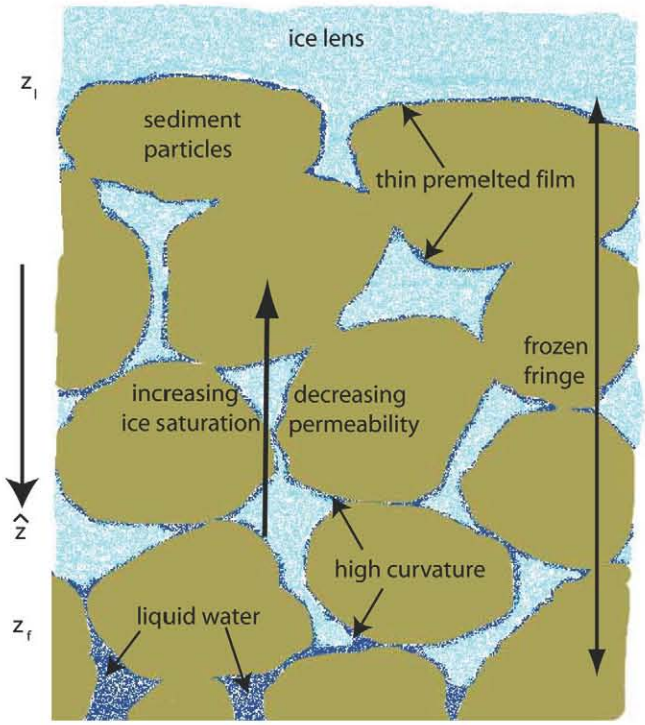

Fig. 4. Schematic diagram showing ice extending beneath an ice-lens boundary at z_l to the bottom of a frozen fringe at z_f (modified from Rempel, 2010).

Net Force Exerted by Sediment Particles on an Active Ice Lens

The elementary example of an ice lens at z_l that is connected through sediments with porosity ϕ by a frozen fringe that extends to a warmer depth z_f helps to build intuition by allowing the net thermomolecular force to be quantified explicitly (see Fig. 4). For this geometry, the net thermomolecular force is the sum of that which would be present on an isolated interface at z_l and that which would be present on an enclosed ice surface that extends through the volume of the frozen fringe. With isotherms running perpendicular to the z axis, and $\hat{\mathbf{z}}$ defined as a unit vector pointing in the direction of increasing temperature, Eq. [8], [9], and [10] can be combined to write

$$\begin{aligned}\mathbf{F}_T &= \frac{\rho_i L A}{T_m}\left[(T_m - T)_l\,\hat{\mathbf{z}} - \frac{T_m}{T_{m0}}\int_{z_l}^{z_f}\phi S_i \mathbf{G}\,dz\right] \\ &\approx \frac{\rho_i L A}{T_{m0}}\hat{\mathbf{z}}\left\{(T_m - T)_l - \right. \\ &\left.\phi\int_{(T_m-T)_f}^{(T_m-T)_l}\left[1-\left(\frac{\Delta T_{f0}}{T_m - T}\right)^{\beta_0}\right]d(T_m - T)\right\}\end{aligned} \quad [11]$$

(Here, the special case is considered in which all ice within the fringe is connected to the lens; if disconnected ice pockets contribute to S_i, the size of the integrand on the right should be reduced accordingly.) Evaluating the integral and defining the undercooling at the lens boundary as $\Delta T_l = T_{m0} - T_l$ gives

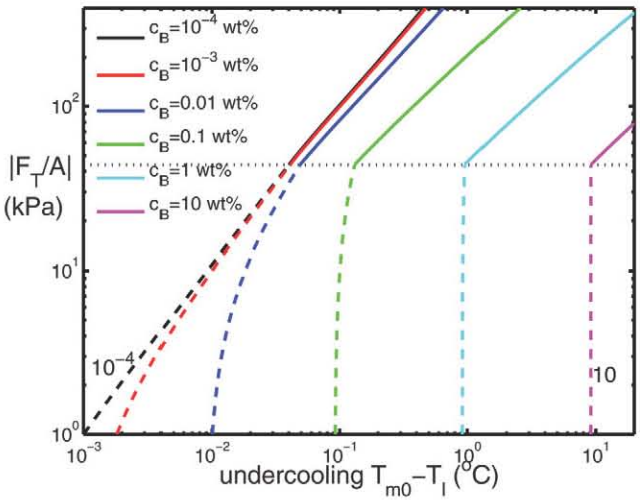

Fig. 5. The thermomolecular force per unit area, $|F_T/A|$, exerted by sediments on an ice lens, plotted as a function of the undercooling on its boundary. Solid lines are for cases with an attached fringe of pore ice extending to warmer temperatures, dashed lines show how $|F_T/A|$ varies when the lens undercooling is too low for ice to form in the adjacent pore space. Plots illustrate cases where the pore space is characterized by the range of bulk impurity concentrations c_B that are shown in the legend. For these calculations, the porosity was taken as $\phi = 0.26$ in Eq. [12] and the saturation behavior was assumed to follow that described in Fig. 2 and 3.

$$\begin{aligned}\mathbf{F}_T \approx -\frac{\rho_i L A}{T_{m0}}\hat{\mathbf{z}}&\left\{\left[\Delta T_l - \Gamma c_B\left(\frac{\Delta T_l}{\Delta T_f}\right)^{\beta}\right]\right. \\ &\left.\times\left[1-\phi+\frac{\phi}{1-\beta_0}\left(\frac{\Delta T_f}{\Delta T_l}\right)^{\beta}\right]-\frac{\phi\beta_0\Delta T_{f0}}{1-\beta_0}\right\}\end{aligned} \quad [12]$$

Figure 5 plots the predictions of Eq. [12] for the magnitude of the thermomolecular force per unit cross-sectional area on an ice lens in the model sediment. Equation [8] was used to extend the curves (with dashed lines) to lens undercoolings lower than ΔT_f (i.e., the regime where no frozen fringe is present). As the undercooling increases, the ice and sediment particles are brought closer together and the stronger intermolecular interactions that result produce an almost linear rise in $|\mathbf{F}_T/A|$ with ΔT_l. The black curve on the far left, plotted for a bulk solute concentration of 10^{-4}% (w/w) is indistinguishable from the predicted behavior with $c_B = 0$. At higher impurity concentrations, there is a corresponding increase in the "initial" liquidus temperature before ice formation with $c = c_B$; the differences between the undercoolings at which each of the dashed curves intersect the abscissa result from this change. Because the pore geometry is fixed, the amount by which curvature effects offset the initial liquidus temperature from the temperature at which pore ice is first able to form (~0.040°C) must be the same for each value of c_B, as is the value of $|\mathbf{F}_T/A| \approx 44$ kPa at which a fringe is first able to form (marked by the dotted line in Fig. 5); this causes the dashed lines that emerge from the abscissa at higher undercoolings to appear to be much steeper on a log–log plot such as this. Comparing the behavior at undercoolings that are large enough for a fringe to form (above the dotted line), $|\mathbf{F}_T/A|$ increases slightly less rapidly when c_B is higher because the dissolved concentration increases as ice fills the pore space, and this lowers the liquidus temperature. As a result, the change to the offset from bulk equilibrium conditions is not as large as it would be if c_B were lower. In Fig. 5, the limit on the ordinate was chosen to focus the display on undercoolings for which the power-law fits give reasonable approximations to the saturation data plotted in Fig. 2. The upper limit on the abscissa was chosen to correspond approximately with the eutectic temperature of NaCl solutions, beyond which a linear extension to the liquidus is not valid.

Liquid Transport through Partially Frozen Sediments

Each line shown in Fig. 5 gives the magnitude of the net thermomolecular force exerted on an ice lens as a function of undercooling at a constant bulk impurity concentration. If the force of gravity on the material above is able to balance this force, less the buoyancy force provided by the surrounding unfrozen liquid in a hydrostatic state, then a static force balance can be achieved in which the lens neither grows nor shrinks but remains in place at a constant undercooling. In order for such a state to be maintained, the rate of heat flow through the adjacent sediments to the ice-lens surface must also exactly balance the rate of heat flow through the lens. This combination of conditions can be achieved, but the natural world

is much more transient and interesting. If there is an imbalance in the heat flow across the lens boundary, for example if the temperature at the ground surface is changing, then melting or freezing must take place at a rate such that latent heat release compensates the difference. The liquid so generated or consumed cannot remain stagnant because saturation levels are fixed by the phase equilibrium conditions. Instead, liquid must flow perpendicular to the lens boundary, and this entails a hydrodynamic pressure gradient, which in turn causes the total fluid force exerted on the lens to be different from its hydrostatic level. Because gravity is inflexible, the lens undercooling must respond and thereby adjust $\mathbf{F}_T$ to maintain the force balance. All of this becomes more involved when impurities are transported in the liquid and ultimately concentrated or diluted as freezing or melting take place, so that $\mathbf{F}_T$ must deviate from the constant-c_B lines shown in Fig. 5. This gives a sense for how the coupled transport of fluid, heat, and solute ultimately control the dynamics of hydromechanical processes in frozen soils. These issues are certainly no less complicated for being familiar from studies of the unsaturated environment.

Extensions

The intent of this contribution has been to concentrate on the more novel physical elements involved in freezing soils. A recent review by Wettlaufer and Worster (2006) provided further background on the fluid mechanical considerations that influence premelting dynamics. Watanabe and Flury (2008) developed an insightful model for the controls on permeability in partially frozen sediments that determine the size of the hydrodynamic force on the lens boundary for a given rate of Darcy flow. Style and Peppin (2012) focused on modifications to the hydrodynamic force that can be important when flow through the premelted films immediately adjacent to a growing lens requires a comparable pressure drop to that required by more large-scale permeable flow. The careful observations and laboratory studies of ice-lens growth in Japan by Mutou et al. (1998) and Watanabe and Mizoguchi (2000) motivated construction of a similar apparatus in the UK that has provided a wealth of new insights into the solidification of colloidal suspensions and the strong analogies with the dynamics of alloy solidification (Peppin et al., 2006, 2007, 2008). Many other contributions have focused on partially frozen soils that are influenced by changing land use and climate in arctic and alpine environments, with implications for major land surface, hydrologic, and biological disruptions (e.g., Forbes, 1999; Matsuoka, 2001; Smith et al., 2005; Williams, 1995).

Summary

Intermolecular forces control phase equilibrium conditions and, in porous media, the proximity of particle surfaces ensures the participation of a different set of interactions that cause the melting temperature to be offset slightly from its bulk value. The pore geometry and mineral surface properties exert a significant control on what that offset is, and soluble impurities are also very important. Practical strategies have been developed for quantifying this behavior to determine how the ice and liquid saturations vary with temperature. Building from a simple example of saturation changes in a two-dimensional model soil, straightforward calculations enable the net force exerted between the ice and particle surfaces to be evaluated. This force is controlled by temperature, whereas the force due to gravity is not; the liquid pressure must adjust to compensate. A vast range of soil freezing phenomena can be traced to the hydromechanical coupling that results.

Acknowledgments

I am grateful to the editors for soliciting this review and giving me the opportunity to share my perspectives and to the reviewers for their insight and help toward improving the final manuscript. My work is funded by NSF ARC-0806355.

References

Abbe, C. 1905. Ice columns in gravelly soil. Mon. Weather Rev. 32:157–158.

Andersland, O.B., and B. Ladanyi. 2004. An introduction to frozen ground engineering, 2nd ed. Chapman and Hall, New York.

Anderson, S.P. 1988. The upfreezing process: Experiments with a single clast. Geol. Soc. Am. Bull. 100:609–621. doi:10.1130/0016-7606(1988)100<0609:TUPEWA>2.3.CO;2

Beskow, G. 1991. Soil freezing and frost heaving with special application to roads and railroads. In: P.B. Black and M.J. Hardenberg, editors, Historical perspectives in frost heave research. CRREL Spec. Rep. 91-23. U.S. Army Cold Reg. Res. Eng. Lab., Hanover, NH. p. 37–157. (Orig. publ. 1935.)

Black, P.B. 1991. Historical perspective of frost heave research. In: P.B. Black and M.J. Hardenberg, editors, Historical perspectives in frost heave research. CRREL Spec. Rep. 91-23. U.S. Army Cold Reg. Res. Eng. Lab., Hanover, NH. p. 1–11.

Cahn, J.W., J.G. Dash, and H.-Y. Fu. 1992. Theory of ice premelting in monosized powders. J. Cryst. Growth 123:101–108. doi:10.1016/0022-0248(92)90014-A

Dash, J.G. 1989. Thermomolecular pressure in surface melting: Motivation for frost heave. Science 246:1591–1593. doi:10.1126/science.246.4937.1591

Dash, J.G., A.W. Rempel, and J.S. Wettlaufer. 2006. The physics of premelted ice and its geophysical consequences. Rev. Mod. Phys. 78:695–741. doi:10.1103/RevModPhys.78.695

Forbes, B.C. 1999. Land use and climate change on the Yamal Peninsula of north-west Siberia: Some ecological and socio-economic implications. Polar Res. 18:367–373. doi:10.1111/j.1751-8369.1999.tb00316.x

Gay, J.-M., J. Suzanne, J.G. Dash, and H.Y. Fu. 1992. Premelting of ice in exfoliated graphite: A neutron-diffraction study. J. Cryst. Growth 125:33–41. doi:10.1016/0022-0248(92)90317-C

Gilpin, R.R. 1979. A model of the "liquid-like" layer between ice and a substrate with applications to wire regelation and particle migration. J. Colloid Interface Sci. 68:235–251. doi:10.1016/0021-9797(79)90277-7

Gilpin, R.R. 1980. A model for the prediction of ice lensing and frost heave in soils. Water Resour. Res. 16:918–930. doi:10.1029/WR016i005p00918

Hallet, B. 1990. Spatial self-organization in geomorphology, from periodic bedforms and patterned ground to scale-invariant topography. Earth Sci. Rev. 29:57–75.

Hallet, B. 2006. Why do freezing rocks break? Science 314:1092–1093. doi:10.1126/science.1135200

Hansen-Goos, H., and J.S. Wettlaufer. 2010. Theory of ice premelting in porous media. Phys. Rev. E 81:031604. doi:10.1103/PhysRevE.81.031604

Ishizaki, T., M. Maruyama, Y. Furukawa, and J.G. Dash. 1996. Premelting of ice in porous silica glass. J. Cryst. Growth 163:455–460. doi:10.1016/0022-0248(95)00990-6

Israelachvili, J. 1992. Intermolecular and surface forces. Academic Press, London.

Krembs, C., H. Eicken, and J.W. Deming. 2011. Exopolymer alteration of physical properties of sea ice and implications for ice habitability and biogeochemistry in a warmer Arctic. Proc. Natl. Acad. Sci. 108:3653–3658. doi:10.1073/pnas.1100701108

Lawler, D.M. 1988. A bibliography of needle ice. Cold Reg. Sci. Technol. 15:295–310. doi:10.1016/0165-232X(88)90076-6

Le Conte, J. 1850. Observations on a remarkable exudation of ice from the stems of vegetables, and on a singular protrusion of icy columns from certain kinds of earth during frosty weather. Proc. Am. Assoc. Adv. Sci. 3:20–34.

Matsuoka, N. 2001. Solifluction rates, processes and landforms: A global review. Earth Sci. Rev. 55:107–134. doi:10.1016/S0012-8252(01)00057-5

Mangold, N., S. Maurice, W.C. Feldman, F. Costard, and F. Forget. 2004. Spatial relationships between patterned ground and ground ice detected by the neutron spectrometer on Mars. J. Geophys. Res. 109:E08001. doi:10.1029/2004JE002235

Maruyama, M., M. Bienfait, J.G. Dash, and G. Coddens. 1992. Interfacial melting of ice in graphite and talc powders. J. Cryst. Growth 118:33–40. doi:10.1016/0022-0248(92)90046-L

Miller, R.D. 1978. Frost heaving in non-colloidal soils. In: Proceedings of the 3rd International Conference on Permafrost, Edmonton, Alberta. 10–13 July 1978. Natl. Res. Counc. Canada, Ottawa, ON. p. 708–713.

Miller, R.D., and E.E. Koslow. 1980. Computation of rate of heave versus load under quasi-steady state. Cold Reg. Sci. Technol. 3:243–251. doi:10.1016/0165-232X(80)90031-2

Murton, J.B., R. Peterson, and J.-C. Ozouf. 2006. Bedrock fracture by ice segregation in cold regions. Science 314:1127–1129. doi:10.1126/science.1132127

Mutou, Y., K. Watanabe, T. Ishizaki, and M. Mizoguchi. 1998. Microscopic observation of ice lensing and frost heave in glass beads. In: A.G. Lewkowicz and M. Allard, editors, Proceedings of the 7th International Conference on Permafrost, Yellowknife, NWT, Canada. 23–27 June 1998. Centre d'etudes nordiques, Univ. Laval, Quebec, QC, Canada. p. 783–787.

O'Neill, K. 1983. The physics of mathematical frost heave models: A review. Cold Reg. Sci. Technol. 6:275–291. doi:10.1016/0165-232X(83)90048-4

O'Neill, K., and R.D. Miller. 1985. Exploration of a rigid ice model of frost heave. Water Resour. Res. 21:281–296. doi:10.1029/WR021i003p00281

Or, D., and M. Tuller. 1999. Liquid retention and interfacial area in variably saturated porous media: Upscaling from single-pore to sample-scale model. Water Resour. Res. 35:3591–3605. doi:10.1029/1999WR900262

Peppin, S.S.L., J.A.W. Elliott, and M.G. Worster. 2006. Solidification of colloidal suspensions. J. Fluid Mech. 554:147–166. doi:10.1017/S0022112006009268

Peppin, S.S.L., J.S. Wettlaufer, and M.G. Worster. 2008. Experimental verification of morphological instability in freezing aqueous colloidal suspensions. Phys. Rev. Lett. 100:238301. doi:10.1103/PhysRevLett.100.238301

Peppin, S.S.L., M.G. Worster, and J.S. Wettlaufer. 2007. Morphological instability in freezing colloidal suspensions. Proc. R. Soc. Ser. A 463:723–733. doi:10.1098/rspa.2006.1790

Peterson, R.A., and W.B. Krantz. 2008. Differential frost heave model for patterned ground formation: Corroboration with observations along a North American arctic transect. J. Geophys. Res. 113:G03S04. doi:10.1029/2007JG000559

Rascón, C., and A.O. Parry. 2000. Geometry-dominated fluid adsorption on sculpted solid substrates. Nature 407:986–989. doi:10.1038/35039590

Rempel, A.W. 2008. A theory for ice–till interactions and sediment entrainment beneath glaciers. J. Geophys. Res. 113:F01013. doi:10.1029/2007JF000870

Rempel, A.W. 2010. Frost heave. J. Glaciol. 56:1122–1128. doi:10.3189/002214311796406149

Rempel, A.W., J.S. Wettlaufer, and M.G. Worster. 2001. Interfacial premelting and the thermomolecular force: Thermodynamic buoyancy. Phys. Rev. Lett. 87:088501. doi:10.1103/PhysRevLett.87.088501

Rempel, A.W., J.S. Wettlaufer, and M.G. Worster. 2004. Premelting dynamics in a continuum model of frost heave. J. Fluid Mech. 498:227–244. doi:10.1017/S0022112003006761

Smith, L.C., Y. Sheng, G.M. MacDonald, and L.D. Hinzman. 2005. Disappearing arctic lakes. Science 308:1429. doi:10.1126/science.1108142

Style, R.W., and S.S.L. Peppin. 2012. The kinetics of ice-lens growth in porous media. J. Fluid Mech. 692:482–498. doi:10.1017/jfm.2011.545

Style, R.W., S.S.L. Peppin, A.C.F. Cocks, and J.S. Wettlaufer. 2011. Ice-lens formation and geometrical supercooling in soils and other colloidal materials. Phys. Rev. E 84:041402. doi:10.1103/PhysRevE.84.041402

Taber, S. 1929. Frost heaving. J. Geol. 37:428–461. doi:10.1086/623637

Taber, S. 1930. The mechanics of frost heaving. J. Geol. 38:303–317. doi:10.1086/623720

Watanabe, K., and M. Flury. 2008. Capillary bundle model of hydraulic conductivity for frozen soil. Water Resour. Res. 44:W12402. doi:10.1029/2008WR007012

Watanabe, K., and M. Ito. 2008. In situ observation of the distribution and activity of microorganisms in frozen soil. Cold Reg. Sci. Technol. 54:1–6. doi:10.1016/j.coldregions.2007.12.004

Watanabe, K., and M. Mizoguchi. 2000. Ice configuration near a growing ice lens in a freezing porous medium consisting of micro glass particles. J. Cryst. Growth 213:135–140. doi:10.1016/S0022-0248(00)00353-5

Watanabe, K., and T. Wake. 2009. Measurement of unfrozen water content and relative permittivity of frozen unsaturated soil using NMR and TDR. Cold Reg. Sci. Technol. 59:34–41. doi:10.1016/j.coldregions.2009.05.011

Wettlaufer, J.S. 1999. Impurity effects in the premelting of ice. Phys. Rev. Lett. 82:2516–2519. doi:10.1103/PhysRevLett.82.2516

Wettlaufer, J.S., and M.G. Worster. 2006. Premelting dynamics. Annu. Rev. Fluid Mech. 38:427–452. doi:10.1146/annurev.fluid.37.061903.175758

Wettlaufer, J.S., M.G. Worster, L.A. Wilen, and J.G. Dash. 1996. A theory of premelting dynamics for all power law forces. Phys. Rev. Lett. 76:3602–3605. doi:10.1103/PhysRevLett.76.3602

Wilen, L.A., and J.G. Dash. 1995. Frost heave dynamics at a single-crystal interface. Phys. Rev. Lett. 74:5076–5079. doi:10.1103/PhysRevLett.74.5076

Williams, P.J. 1995. Permafrost and climate change: Geotechnical implications. Philos. Trans. R. Soc. London, Ser. A 352:347–358. doi:10.1098/rsta.1995.0075